IEEE Geoscience and Remote Sensing Letters,
July 2013, Volume 10, Issue 4, Pages 761-765
http://dx.doi.org/10.1109/LGRS.2012.2222341

On Dual Co-Polarized SAR Measurements of the Ocean Surface

V.N. Kudryavtsev[a], B. Chapron[b], A.G. Myasoedov[a], F. Collard[c] and J.A. Johannessen[d]

[a] Satellite Oceanogr. Lab. (SOLab), Russian State Hydrometeorological Univ., St. Petersburg, Russia
[b] Institute Francais de Recherche pour l'Exploitation de la Mer, 29280 Plouzané, France.
[C] Division of Radar Applications, CLS, 29280 Plouzané, France.
[d] Nansen Environmental and Remote Sensing Center, 5006 Bergen, Norway.

*: Corresponding author : V.N. Kudryavtsev, email address : e-mail: kudr@rshu.ru

Abstract:

An effective methodology using satellite high-resolution polarized information to interpret and quantitatively assess various surface ocean phenomena is suggested. Using a sample RADARSAT-2 quad-polarization ocean synthetic aperture radar (SAR) scene, the dual co-polarization (VV and HH) radar data are combined into polarization difference, polarization ratio, and nonpolarized components. As demonstrated, these field quantities provide means to distinguish Bragg scattering mechanism and radar returns from breaking waves. As shown, quantitative characteristics of the surface manifestation of ocean currents, slicks, and wind field features in these dual co-polarization properties are very different and may be effectively used in the development of new SAR detection and discrimination algorithms.

Keywords: Radar cross sections ; radar signal analysis ; synthetic aperture radar (SAR) imaging

I. Introduction

The goal of this this study is to promote a very effective methodology using satellite high resolution dual copolarized information to interpret and quantitatively assess various surface ocean phenomena. Spaceborne synthetic aperture radar (SAR) has already proven to be a very useful tool to assess and reveal various ocean–atmosphere processes (see, e.g., [1]). Accordingly, methods have been demonstrated to advance quantitative interpretations of the SAR image intensity contrasts associated with local ocean surface roughness variations linked to changes in the near-surface winds, waves, and currents, as well as the presence of surface contaminants.

With the advent of new SAR instrument systems, dual- and quad-polarization SAR data are now made available, to possibly yield more useful information than conventional single polarization SAR observations. This can help to possibly go beyond the present geophysical retrieval algorithms. For instance, Zhang *et al.* [2] demonstrated such a new potential to map oil slick using polarimetric SAR decomposition parameters obtained from a RADARSAT-2 quad-polarization image. Indeed, as previously suggested by Schuler and Lee, ambient clean sea and slick areas can be well separated using the polarimetric matrix decomposition, particularly suggesting that non-Bragg scattering becomes dominant over oil slicks.

However, without taking into account the full amplitude and phase information of each resolved pixel of quad-polarization observations, dual co-polarized radar instrument could be already ideally suited. As analyzed by Mouche *et al.*, copolarized VV and HH data can be combined to infer both local wind characteristics and then minimize the wind-induced surface motion to estimate surface current. According to different asymptotic electromagnetic models, the polarization sensitivity for both Doppler shifts and radar intensity signals seems readily exploitable. The combined use of dual co-polarized measurements can then become a very efficient tool to better understand, discriminate, and quantify the different scattering mechanisms responsible for the manifestation of surface currents, slicks, and wind field features in SAR images.

In this letter, the proposed methodology is tested and assessed with a RADARSAT-2 fine-mode quad-polarization SAR image, but we solely focus on the dual co-polarized VV and HH products. Hereafter, we take advantage of this dual information to effectively and quickly identify different scene areas where wind direction changes occur or where surface wave–current interactions strongly enhance surface breaking waves. The proposed methodology also helps to identify and interpret oil spill manifestations, to possibly complement analysis using the full-polarimetric SAR information.

II. Observations and interpretation

A. SAR Data

This study is based on a quad-polarized RADARSAT-2 SAR image acquired over the Mediterranean Sea, i.e., the coastal area near the town of Begur (Spain), which is acquired at 17:40 UTC on December 18, 2010 (see Fig. 1). The SAR image roughly covers a 40 km × 50 km area and has pixel spacing of about 5 and 10 m in slant and azimuth directions, respectively.In this image, the incidence angle varies from 32.7° to 35.7°. The RADARSAT-2 Wide Fine Quad-Pol imaging mode provides single-look complex data in HH, HV, VH, and VV polarizations. VV- and HH-polarized images are shown in Fig. 1(a) and (b). The corresponding image of the polarization ratio (HH over VV in linear units, hereinafter PR) and the polarization

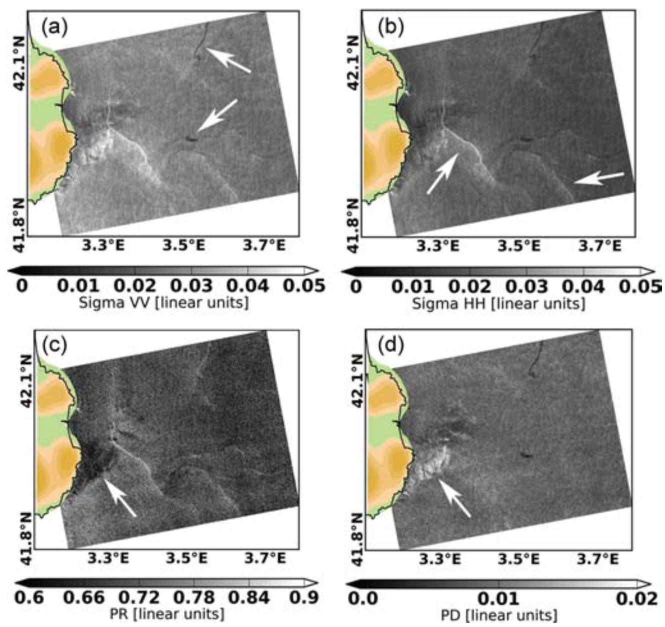

Fig. 1. RADARSAT-2 SAR image of a coastal area in the Mediterranean Sea acquired at 17:40 UTC on December 18, 2010 in terms of (a) VV-polarization, i.e., σ_0^{vv} (in linear units); (b) HH-polarization, i.e., σ_0^{hh}; (c) PR $\sigma_0^{\mathrm{hh}}/\sigma_0^{\mathrm{vv}}$ (in linear units); and (d) PD $\Delta\sigma = \sigma_0^{\mathrm{vv}} - \sigma_0^{\mathrm{hh}}$ (in linear units). The arrows indicate manifestations of (a) surface slicks, (b) surface current signatures, and (c) and (d) wind field features.

difference (VV minus HH in linear units, hereinafter PD) are shown in Fig. 1(c) and (d), respectively. It was checked that signal intensity is everywhere ten times above the thermal noise level, even for HH signals over the reduced backscatter slick areas. As such, it was not necessary to account for the thermal noise in the normalized radar cross section (NRCS) calibration and subsequent PR and PD calculations.

Fig. 2(a) provides Meteo-France AROME model information about the surface wind field conditions. Mostly blowing from the south, an offshore wind has developed near the coast, with chances of convective clouds and associated rain cells at the atmospheric front, as seen on the SAR scenes. The Doppler frequency shift in Fig. 2(b) confirms the near-coastal wind direction change predicted by the atmospheric model.

In Fig. 1(a) and (b), both VV and HH SAR images exhibit distinct linear bright/dark signatures, which can be interpreted as manifestations of surface currents, and two dark areas presumably caused by the surface slicks. The distinct current-induced features are well expressed in the PR field but almost entirely removed in the PD field (see Figs. 1 and 4). The clear drop of the Doppler velocity in Fig. 2(b) across the bright SAR signatures confirms that this signature traces the surface current shear. Unlike the current-induced features, the surface slicks are detected in both PR and PD fields. However, within the slicks, the PR values are larger over the ambient area, whereas PD values are lower to reflect the surface roughness suppression in the slicks (see Figs. 1 and 3).

B. Model Approach

To interpret these observed SAR features, the HH and NRCS components are represented as a sum of polarized scattering, which is associated with the conventional two-scale Bragg scattering σ_{0B}^{pp} and the nonpolarized (NP) scattering from breaking waves σ_{wb} [5], [6], i.e.,

$$\sigma_0^{pp} = \sigma_{0B}^{pp} + \sigma_{\mathrm{wb}}. \tag{1}$$

The NP scattering originates from radar returns from very "rough" and "steep" surface patches, and it is the same at both polarizations (see, e.g., [5], [7], and corresponding references). Using the NRCS model (1), the PR reads

$$P \equiv \frac{\sigma_0^{\mathrm{hh}}}{\sigma_0^{\mathrm{vv}}} = \frac{\sigma_{0B}^{\mathrm{hh}} + \sigma_{\mathrm{wb}}}{\sigma_{0B}^{\mathrm{vv}} + \sigma_{\mathrm{wb}}}. \tag{2}$$

PR values have already received attentions reported in the literature, mostly to discuss departure from tilted Bragg scattering mechanism due to the impact of breaking waves (see, e.g., [7] and [8]). In particular, Mouche *et al.* reported comprehensive analysis of dual-polarized C-band airborne radar measurements and found a remarkable deviation of the observed PR values from the Bragg scattering predictions, showing, in turn, significant contribution of the NP scattering to the sea surface NRCS.

The wave breaking contribution can be thus removed using the PD between VV and HH NRCSs, i.e.,

$$\Delta\sigma_0 \equiv \sigma_0^{\mathrm{vv}} - \sigma_0^{\mathrm{hh}} = \sigma_{0B}^{\mathrm{vv}} - \sigma_{0B}^{\mathrm{hh}} \tag{3}$$

which is controlled by the surface roughness produced by wave components close to the Bragg wave number. Since C-band Bragg waves, which are around 5-cm wavelength, have "quick response" to wind forcing, with the spatial relaxation scale of an order of 10 m, we can anticipate that PD $\Delta\sigma_0$ should closely reflect the near-surface wind variability and presence of the slicks.

From (1) and (3), the NP component, i.e., σ_{wb}, can be assessed as

$$\sigma_{\mathrm{wb}} = \sigma_0^{\mathrm{vv}} - \Delta\sigma_0/(1 - p_B) \tag{4}$$

where p_B is the PR for the two-scale Bragg scattering, i.e.,

$$p_B = \sigma_{0B}^{\mathrm{hh}}/\sigma_{0B}^{\mathrm{vv}}. \tag{5}$$

For the two-scale Bragg scattering, p_B is mostly governed by the local geometry and tilting effects. At moderate incidence angles, i.e., $\theta > 25^\circ$, relation for p_B can be simplified to (see, e.g., [7, eq. (31)])

$$p_B = \frac{|G_h|^2}{|G_v|^2}\left[1 + (g_h - g_v)s_i^2\right] \tag{6}$$

where $|G_p|$ is the scattering coefficient (depending on the incidence angle), $g_p = 1/2 \cdot \partial^2|G_p|/\partial^2\theta$, and s_i^2 is the mean square slope of tilting waves (waves with wavelength longer than few times the Bragg wavelength) in the incidence plane direction. The second term in the square bracket describes the impact of tilting waves to p_B. In the range of incidence angles from 25° to 45°, it varies from 0 (calm) to about 0.5 at moderate winds. Thus, p_B may be assumed to be weakly dependent on wind speed and almost independent on azimuth (due to

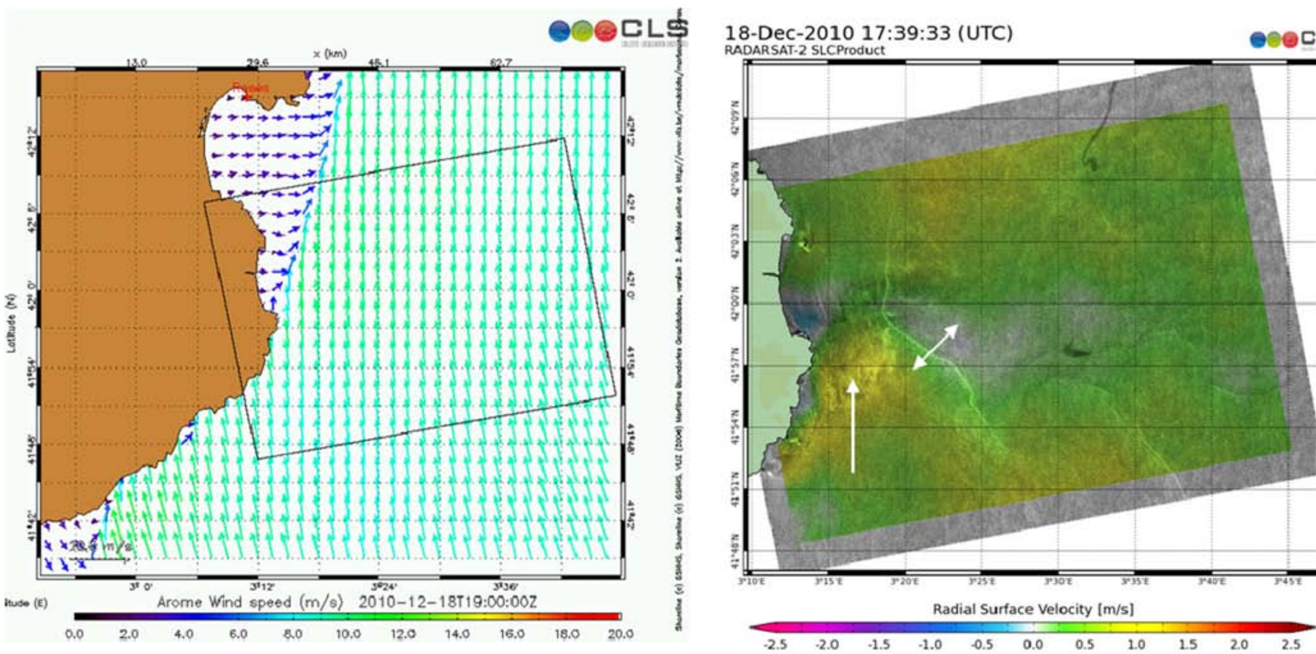

(a) (b)

Fig. 2. (a) Contemporaneous Meteo-France AROME model surface wind field. (b) Doppler velocity field overlapped the VV NRCS image. The box in (a) indicates the position of the SAR image. The positive Doppler velocity is directed toward the SAR look direction. The arrow in (b) indicates the area with "large" positive values of Doppler velocity spatially coincident with the manifestation of the wind field feature marked in Fig. 1(c) and (d). The double-sided arrow marks the Doppler velocity drop over the bright NRCS signature. Near the coastal area, the Doppler changes sign to confirm the wind direction change becoming downwind, where the Doppler is negative. Over the main area, the Doppler values are small, confirming crosswind radar conditions.

approximately azimuthal isotropy of tilting waves slopes; see also [8, Fig.16]). For the considered RADARSAT-2 image, two-scale model simulations give p_B to vary from 0.56 to 0.45 in linear units for incidence angles ranging from 32.7° to 35.7°.

Based on model (1), the original co-polarized VV and HH images can be thus transformed to new PD and NP images defined by (3) and (4), respectively, which possess information on very different radar scattering mechanisms, i.e., the polarized Bragg scattering provided by short fast-response wind waves and NP radar returns from breaking waves in a wide spectral range. Interplay between these mechanisms is included in the PR image defined by (2). Due to different sensitivity of short wind waves and wave breaking to various ocean phenomena, this set of new images can then serve as an effective tool for SAR data interpretation.

C. Scattering Mechanism Analysis

In the present case, the mean PR is about 0.7 in linear units [about -1.5 dB; see Fig. 1(c)], except within the "dark" area near the coast [see the arrow in Fig. 1(c)], where PR drops to 0.55 (or about -2.5 dB). In this area, the wind direction is offshore, close to the downwind radar look direction. In the downwind direction, the model suggests that the Bragg component dominates over the wave breaking contribution that results in a lower PR (see also , Fig. 16[8]). In addition to the atmospheric model [see Fig. 2(a)], the offshore wind direction in this area is also confirmed by the positive Doppler velocity [see Fig. 2(b)]. In this localized coastal area, the PR values are in closer agreement with the two-scale Bragg scattering model. Outside this coastal area, the PR values are larger, about 0.7, confirming the significant contribution of wave breaking to the total NRCS (about 40%).

The bright/dark quasi-linear current-induced signature in the PR field (see Figs. 1(c) and 4) can be further interpreted as enhancement/suppression of wave breaking due to wave–current interactions. As found, the PR values related to this bright quasi-linear feature are close to 1 in linear units (0 dB), indicating that NRCS is mostly dominated by rough patches of breaking waves, and the effect of Bragg wave modulation by current is negligible.

Over the slick area, PR values are also larger than the background values (see Fig. 3). Surface films (either biogenic or oil) suppress short wind waves and thus reduce resonant Bragg scattering (see, e.g., [9]). However, wind waves with wavelength on the order of a decimeter and longer are not damped by the surface films. Hence, the contribution of these longer waves within slicks is probably the same as outside, leading to increased PR values (see Fig. 3).

D. Polarization Decomposition

As anticipated, a PD image should closely reflect the near-surface wind variability and slicks. Near the coast, where off-shore winds are expected due to breezes, the NRCS difference is clearly enhanced [see Fig. 1(d)], confirming a downwind radar look direction, for which Bragg scattering is maximal.

Fig. 1 suggests that the bright/dark quasi-linear feature (associated with the surface currents manifestation) well visible in VV, HH, and PR scenes is not distinguishable in the PD scene (see also Fig. 4). This indicates that SAR signatures over oceanic fronts mostly result from enhanced/suppressed wave

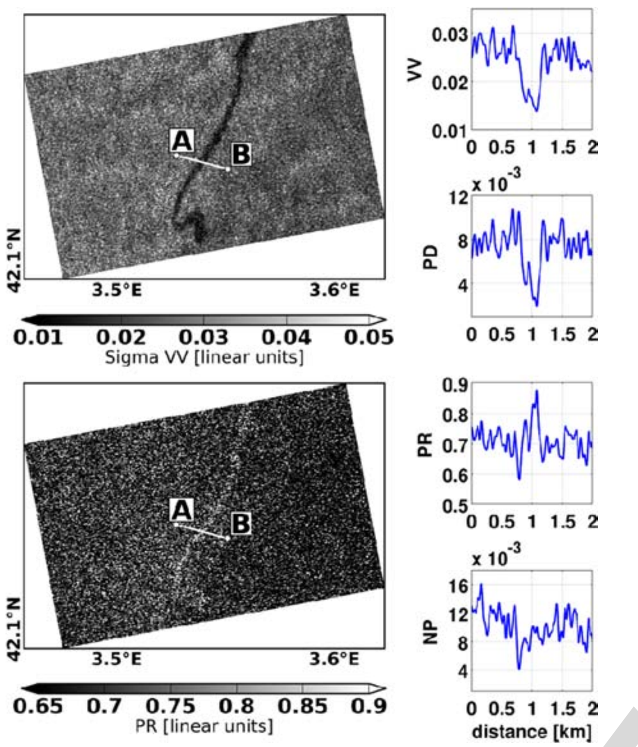

Fig. 3. (Upper left) Enlarged fragment of the slick area in Fig. 1(a). (Lower left) Corresponding enlargement of the PR in Fig. 1(c), showing the same slicks, which manifests as a bright area. (Right column) Cross section across the slick area along line A-B for (top to bottom) VV NRCS $\sigma_0^{\rm vv}$, PR $\sigma_0^{\rm hh}/\sigma_0^{\rm vv}$, PD $\Delta\sigma = \sigma_0^{\rm vv} - \sigma_0^{\rm hh}$, and NP component $\sigma_{\rm wb}$ of the NRCS defined by (4). All quantities are represented in linear units.

breaking, which provide NP radar returns. On the other hand, the slick areas correspond to dark areas due to strong damping of the Bragg waves (see Figs. 1(d) and 3). Notice that the background-to-slick ratio for the PD is about 3 (or 4.8 dB), whereas that for the VV NRCS is only about 1.8 (or 2.6 dB). This shows that PD $\Delta\sigma_0$ is more sensitive to the presence of the surface slick, in comparison with $\sigma_0^{\rm vv}$, as removal of $\sigma_{\rm wb}$ is less affected by slicks. The PD thus contains information about "fast-response" spatial changes of short-scale Bragg waves, which are mainly caused by variable wind field and/or the presence of surface slicks.

E. Wave Breaking Contribution

NP component of the NRCS defined by (4) is shown in Figs. 4 and 5, using $p_B = 0.5$. First, the surface currents' features are remarkably emphasized. The current-over-background ratio for $\sigma_{\rm wb}$ is about 4 (6 dB), which is significantly larger than the similar ratio for VV, which is about 1.6 (or 2 dB). Second, surface slicks are almost not detected in the NP field (see Fig. 3). This indicates that, unlike Bragg waves, longer scale roughness is less affected by slicks, although some small suppression of $\sigma_{\rm wb}$ in the slick area can be revealed.

Near the coast where the wind is blowing offshore, the impact of wave breaking to the NRCS is also noticeably weaker. Such lower values of $\sigma_{\rm wb}$ in this area may partly result from azimuthal dependence of $\sigma_{\rm wb}$. Following [7], the radar return from breaking waves is maximal in the upwind direction

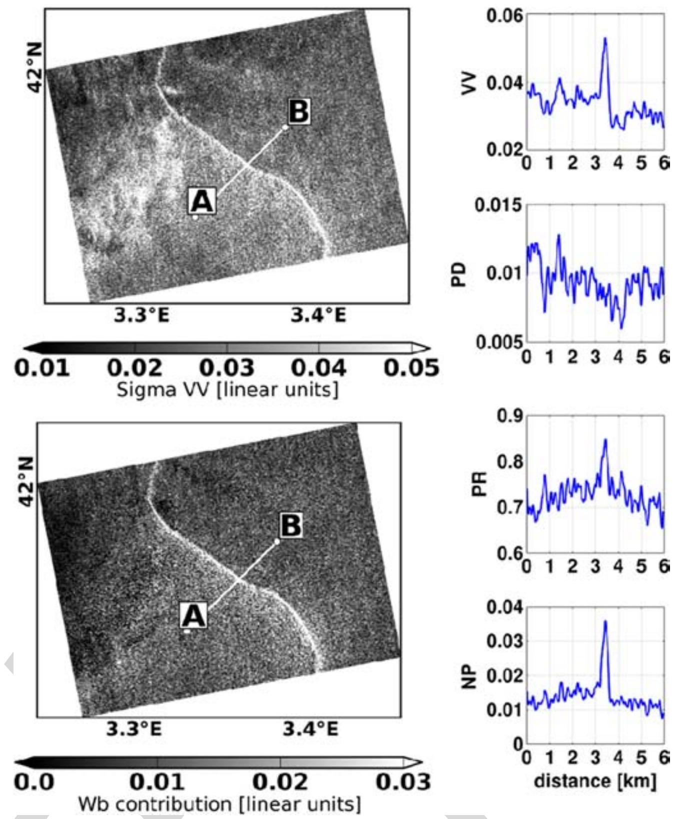

Fig. 4. (Upper left) VV SAR image enlargement of the current feature in Fig. 1(a). (Lower left) NP part of the NRCS of the same signature. (Right column) Cross section across the current feature along line A-B for (top to bottom) VV NRCS $\sigma_0^{\rm vv}$, PR $\sigma_0^{\rm hh}/\sigma_0^{\rm vv}$, PD $\Delta\sigma = \sigma_0^{\rm vv} - \sigma_0^{\rm hh}$, and NP part $\sigma_{\rm wb}$ of the NRCS defined by (4). All quantities are represented in linear units.

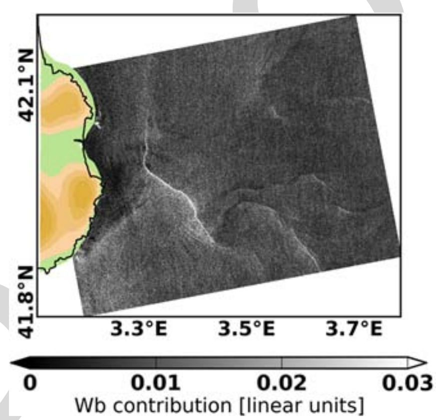

Fig. 5. Wave breaking contribution (NP component of the NRCS) estimated from (4) via $\sigma_0^{\rm vv}$ and $\Delta\sigma_0$ fields shown in Fig. 1.

and minimal in the downwind direction. Analysis of NSCAT Ku-band dual-polarized satellite data also confirms this assumption [6], [10]. Lower values of both $\sigma_{\rm wb}$ and PR near the coast represent a consistent pattern caused by local offshore wind condition. Notice that shorter fetch in the offshore wind area can also lead to lower longer wave contribution, which reduces the NRCS and, more specifically, its NP part. AQ7

III. CONCLUSION

Dual co-polarization SAR data can thus provide a tool to distinguish between different mechanisms affecting ocean radar backscatter. NRCS difference between VV and HH co-polarized data (PD image) enhances variability produced by the resonant scattering mechanism. Since short Bragg waves are "fast-response" waves, a PD image carries information on the spatial variability of surface wind velocity field (including gustiness) and surface slicks.

As demonstrated, combination of VV and PD images can be then used to derive the NP component of the NRCS (NP image), essentially dominated by breaking waves. Since wave breakings are very sensitive to the nonuniform surface current, an NP image shall reflect surface manifestations of sub- and mesoscale ocean currents.

The use of the PD and NP images per se or in their combination with original VV- and HH-images or/and a PR image can thus become a very powerful tool for detection and discrimination of various ocean surface phenomena such as surface currents, slicks, and wind field features.

Over the main area of the radar scene considered in this letter, the radar look direction corresponds to the crosswind direction. As have been shown by Kudryavtsev *et al.*, such observation geometry is optimal for SAR detection of surface current features, which are distinctly visible in both VV and HH images as linear bright/dark features linked to the surface current velocity gradients identified via Doppler velocity measurements. As even better detected in the NP image, the origin of such SAR signatures is associated with the enhancement/suppression of wave breaking by the surface current shear. Remarkably, the surface currents are then not visible in the PD image, confirming that the resonant Bragg waves have very short relaxation time and, thus, are not modulated by the surface currents.

The surface slicks are manifested as dark areas in both VV and HH SAR images due to the damping of the Bragg waves. However, slicks appear as "bright" areas in PR images. Though short waves are damped, the radar return supported by longer wave breaking is almost unaffected in slicks. As a result, slicks are well visible in the PD image and almost not visible in NP images. Moreover, the apparent difference of slick signatures in VV image (HH image) and in the PR image opens a promising opportunity to discriminate slicks from a look-alike feature associated with low-wind conditions and surface current effects. This result is in line with the previously reported full-polarimetric analysis [2], [3].

Wind speed variability is well traced in both the PD image and from the Doppler frequency. Wind variability can be thus more effectively "filtered out" from dual co-polarized SAR images to help remove the wind-wave-induced Doppler contribution in [12] to better quantify the surface current signatures in the NP image. In addition, strong azimuthal wind dependence of PR and NP signals may serve as an indicator of wind direction changes. In this study, this feature helped to reveal a localized zone with offshore winds. Future investigations shall further dwell on the present analysis of dual co-polarized SAR data to confirm the radar backscatter polarization sensitivity and to better assess the Doppler frequency polarization sensitivity. As foreseen, combined dual co-polarized SAR data can then help and refine the interpretation of the various detected features (wind field changes, surface currents, and oil slicks versus their look-alikes).

ACKNOWLEDGMENT

The authors would like to thank the support from the SeaU EU FP7 Project 263246 and ANR-BLAN-0365 REDHOTS. AQ8 RADARSAT is an official mark from the Canadian Space Agency (CSA). RADARSAT-2 SAR (CSA) data were acquired within the framework of the VIGISAT project, in the framework of a FEDER Grant Présage No. 32635, and a partnership with CLS for providing the data, under Contracts 08 GET 13M and 09 GET 11M.

REFERENCES

[1] B. Holt, "SAR imaging of the ocean surface," in *Synthetic Aperture Radar Marine User's Manual*, C. R. Jackson and J. R. Apel, Eds. Silver Spring, MD: NOAA, 2004, pp. 263–275.

[2] B. Zhang, W. Perrie, X. Li, and W. G. Pichel, "Mapping sea surface oil slicks using RADARSAT-2 quad-polarization SAR image," *Geophys. Res. Lett.*, vol. 38, no. 10, p. L10 602, May 2011.

[3] D. L. Schuler and J. S. Lee, "Mapping ocean surface features using biogenic slick-fields and SAR polarimetric decomposition technique," *Proc. Inst. Elect. Eng.—Radar Sonar Navig.*, vol. 153, no. 3, pp. 260–270, Jun. 2006.

[4] A. A. Mouche, B. Chapron, N. Reul, and F. Collard, "Predicted Doppler shifts induced by ocean surface wave displacements using asymptotic electromagnetic wave scattering theories," *Waves Random Complex Media*, vol. 18, no. 1, pp. 185–196, Feb. 2008.

[5] O. M. Phillips, "Radar returns from the sea surface—Bragg scattering and breaking waves," *J. Phys. Oceanogr.*, vol. 18, no. 8, pp. 1065–1074, Aug. 1988.

[6] Y. Quilfen, B. Chapron, A. Bentamy, J. Gourrion, T. El Fouhaily, and D. Vandemark, "Global ERS 1 and 2 and NSCAT observations: Upwind/crosswind and upwind/downwind measurements," *J. Geophys. Res.*, vol. 104, no. C5, pp. 11 459–11 469, May 1999.

[7] V. N. Kudryavtsev, D. Hauser, G. Caudal, and B. Chapron, "A semiempirical model of the normalized radar cross-section of the sea surface 1. Background model," *J. Geophys. Res.*, vol. 108, no. C3, pp. 8054–8077, Jan. 2003.

[8] A. A. Mouche, D. Hauser, and V. Kudryavtsev, "Radar scattering of the ocean surface and sea-roughness properties: A combined analysis from dual-polarizations airborne radar observations and models in C band," *J. Geophys. Res.*, vol. 111, no. C9, p. C09 004, Sep. 2006.

[9] M. Gade, W. Alpers, H. Huehnerfuss, H. Masuko, and T. Kobayashi, "Imaging of biogenic and anthropogenic ocean surface films by the multifrequency/multipolarization SIR-C/X-SAR," *J. Geophys. Res.*, vol. 103, no. C9, pp. 18 851–18 866, Aug. 1998.

[10] B. Chapron, V. Kerbaol, and D. Vandemark, "A note on relationships between sea-surface roughness and microwave polarimetric backscatter measurements: Results from POLRAD'96," presented at the Proc. POLRAD Int. ESA Workshop, ESTEC, Noordwijk, The Netherlands, Apr. 29, 1997, ESA WPP-135.

[11] V. N. Kudryavtsev, D. Akimov, J. A. Johannessen, and B. Chapron, "On radar imaging of current features: 1. Model and comparison with observations," *J. Geophys. Res.*, vol. 110, no. C7, p. C07 016, Jul. 2005.

[12] B. Chapron, F. Collard, and F. Ardhum, "Direct measurements of ocean surface velocity from space: Interpretation and validation," *J. Geophys. Res.*, vol. 110, no. C7, p. C07 008, Jul. 2005.